A Full PIC Study of the Neutralization of the RIT10-EVO's Plasma Plume

IEPC-2024-472

Presented at the 38th International Electric Propulsion Conference, Toulouse, France
June 23-28, 2024

Matteo Guaita* and Alberto Marin-Cebrián † and Mario Merino‡ and Eduardo Ahedo§
Department of Aerospace Engineering, Universidad Carlos III de Madrid, Leganés, Spain

and

Fabrice Cipriani¶ and Käthe Dannenmayer‖
European Space Research and Technology Center, ESA, Noordwjik, Netherlands

Numerical simulations of Gridded Ion Thruster plumes are fundamental in the understanding of the plume's properties and interaction with the surrounding environment, as well as for the quantification of the facility effects that may alter the in-space plasma response with respect to the one measured on ground. However, the processes that govern the neutralization of the thruster's ion beam by means of the electrons emitted by an externally mounted cathode, and the appropriate way to account for them both in numerical and experimental works, are still a matter of research in the community. For these reasons this study presents simulations of the plasma plume of Ariane's RIT10-EVO, carried out with a planar, full-PIC code provided of an extensive library of electron, ion and neutral collisions. In particular, we find that the inclusion of electron inelastic collisions such as ionization and excitation results fundamental in the generation of a population of electrons trapped in the plume's potential well, and which play a major role in the neutralization of the plume and in the definition of the electric potential map. This trapped population results mostly insensitive to the emission properties of the neutralizer, but displays a slow approach to stationary conditions dictated by the frequencies of the inelastic collisions included in the simulation. Finally, we also present an axisymmetric simulation case with an annular cathode, that allows the evaluation of a three-dimensional expansion process. The build up of the trapped electron population in this case is even slower, because of the smaller neutral density observed when expanding the plume in three dimensions. However, the main governing physical processes observed in the planar case remain prominent also in this case.

I. Introduction

Gridded Ion Thrusters (GITs) are a vastly employed form of electric propulsion, principally because of their high specific impulse ($I_{sp} > 3000\,\mathrm{s}$) and large flight heritage.[1] These kind of thrusters extract and strongly accelerate an ion beam from a plasma source through a system of electrically biased grids, which is neutralized downstream by means of an electron current emitted by a cathode. This allows to close the electric circuit, producing a current-free plume and avoiding the charging of the thruster and spacecraft.[2]

*PhD student, Equipo de Propulsion al Plasma, mguaita@pa.uc3m.es.
†PhD student, Equipo de Propulsion al Plasma, amarinc@pa.uc3m.es.
‡Permanent Professor, Equipo de Propulsion al Plasma, mario.merino@uc3m.es.
§Permanent Professor, Equipo de Propulsion al Plasma, eahedo@ing.uc3m.es.
¶Space Environment and Effects Analyst, European Space Research and Technology Center, Fabrice.Cipriani@esa.int.
‖Electric Propulsion Engineeer, European Space Research and Technology Center, Kathe.Dennenmayer@esa.int.

Although GITs are a mature technology and the final neutralization of the thruster plume is readily obtained in practice, the theoretical understanding of the coupling between the positive ion beam and the negative electron cloud that allows it is still a matter of research.[3] Moreover, the experimental quantification of their lifespan, and the characterization of their plume and of its possible interaction with the hosting spacecraft, is still hindered by the uncertainties linked to the extrapolation of testing conditions in on-ground vacuum chambers to the in-space environment, commonly termed as 'facility effects'.[4] Of these the most prominent are (i) the presence of a background population of neutral particles in vacuum chamber experiments, that may alter the plume characteristics through collisional processes, and (ii) the chamber walls, that impose a finite dimension of the plume expansion and provide additional conductive paths for the closure of the electric currents.

Model	Authors	Ref.	Year	Ions	State	Conditions	Collisions	Cathode
Hybrid	Korkut	[5–8]	2014-2017	Xenon	Steady	Both	CEX, MEX	Both
	Cichocki	[9]	2017	Xenon	Steady	In-Space	CEX,MEX,el	External
PIC	Usui	[10]	2013	Hydrogen	Transient	In-Space	None	External
	Hu, Wang	[11–14]	2014-2017	Hydrogen	Transient	Both	None	Co-located
	Nuwal	[15]	2020	Xenon	Steady	Chamber	CEX,MEX	External
	Jambunathan	[16–19]	2017-2020	Xenon	Steady	Both	CEX,MEX	Both
	Nishii	[20]	2023	Xenon	Steady	Chamber	CEX,MEX	Co-located
	Nishii	[3]	2023	Xenon	Steady	Both	CEX,MEX	External
Particle-Particle	Zhao	[21]	2018	Xenon	Transient	In-Space	None	Both

Table 1: Summary of previous numerical works on GIT plumes.

Numerous numerical investigations have tackled these topics in the last decade, preciously increasing our understanding of the GIT plume, its dynamics and its response to facility conditions. A non-extensive summary of these works, specifying the type of numerical model that was employed and the main characteristics of the physics that were simulated, is presented in Table 1. The first studies to investigate the steady-state properties of GIT plumes employed hybrid fluid/PIC codes,[5–9] that through a particle description of the heavy species and a fluid model for electrons, together with the assumption of quasi-neutrality, allowed a reduction of the computational costs and the achievement of steady-state. This approach was useful for a first qualitative study of the effects of ion-neutral resonant charge exchange (CEX) collisions, that generate the characteristic high-density lateral wings around GIT plumes. Additionally, these studies allowed a preliminary investigation of the effect of the electrostatic field, responsible for determining the ion backflow to the thruster and the gradual divergence of the plume. However, the body of work by Wang and Hu[11–14] on co-located plasma sources (i.e. ions and electrons were emitted by the same injection surface), together with the later studies of Nuwal and Jambunathan,[15–17] demonstrated the importance of electron kinetics in the retrieval of the electric potential map, and the accurate evaluation of the electric forces acting on ions. Simultaneously, the problem of the ion beam neutralization by means of electrons emitted by an externally located cathode was tackled by Usui and Zhao[10,21] with fully kinetic and non-neutral codes, highlighting the strong non-neutrality of the problem and the presence during the initial transient of axial and radial electron density waves, caused by the bouncing motion of electrons trapped in the potential well generated by the positive ion beam. However, these studies only concentrated on the initial transient, as steady-state conditions for fully kinetic simulations of GIT plumes have been obtained only recently, thanks to the heavy parallelization of modern Particle in Cell (PIC) codes and the introduction of energy-based boundary conditions for electrons.[18,22–24]

With the aid of PIC simulations, the recent works by Jambunathan and Nishii[3,18–20] have explored the dependence of the steady-state conditions of a GIT plume on facility effects and cathode properties. This allowed a precise determination of the energy of backstreaming ions, and the alteration of the densities in the facility, caused by the neutralization of the plasma beam at the chamber walls and their sputtering by high-energy ions. Interestingly, all simulation cases with an externally located cathode (thus simulating the neutralization process of the plasma plume) displayed values of the electric potential and electron temperature in front of the thruster grids that were several times higher than what is observed in experimental measurements.[25] As we propose to show in this work, this was likely caused by the exclusion of inelastic electron collisions in the simulated physics, that would provide an energy sink for the electron population

and, in the case of ionization, also introduce a new source of low energy electrons capable of decreasing the positive space charge of the ion plume.

To the authors' knowledge no fully kinetic, steady-state study of a GIT plume that includes an extensive library of electron and ion collisions has been carried out yet. Additionally, the direct comparison of simulations of GIT plumes with experimental data, that would allow the validation of numerical results, are scarce in the literature. In this work, therefore, we present the steady-state, kinetic and collisional simulations of the plume of Ariane's RIT10-EVO thruster, currently under experimental characterisation at the Justus Liebig Universität (JLU) in Gießen.[26] Because the inclusion of a set of inelastic collisions for electrons is expected to provide an additional mechanism for the trapping of electrons in the plume's potential well, we also propose here a subdivision of the electron particles into distinct 'trapped' and 'free' populations, allowing the independent study of their macroscopic properties.

The remainder of this article is structured as follows. Section II describes the methodology followed for the presented simulations, detailing the properties of the in-house code PICASO and the assumptions and numerical choices involved. Section III then presents a reference simulation and the general plasma response that it provides, which is further analysed in Section IV by detailing the properties of the separate electron classes. A sensitivity analysis on the free parameters of the model and on the effects of electron collisionality is next presented in Section V, while the approach to an axisymmetric simulation and its preliminary results are described in Section VI. Finally, Section VII summarizes the main contributions and results of this work.

II. Methodology

Three distinct codes were employed to obtain the simulations presented and discussed in this work. Firstly, the hybrid in-house code EP2PLUS was used to obtain the steady-state maps describing the population of neutral atoms present in the experimental facility. These were then loaded in the planar version of the full PIC code PICASO, which was used for an initial evaluation of a bi-dimensional plume expansion, thus allowing the study of asymmetrical effects caused by the externally mounted cathode. The planar version of the code was also employed for a sensitivity analysis carried out on some of the most uncertain input parameters. Finally, the axisymmetric version of PICASO permitted the simulation and study of a three-dimensional expansion of the plume, at the price of a loss in the capability to include effects linked to the asymmetry of the physical geometry of the problem. The general properties of the simulation domain and input parameters were kept identical throughout all three codes (with some obvious exceptions linked to the axisymmetrical version, which will be commented later), and are therefore presented collectively in the next Section.

A. The Simulation Domain

Figure 1 presents the simulation domain employed for this study. The domain considered reproduces, within the possibility of the spatial discretization employed, the physical geometry of Ariane's RIT10-EVO. All simulations discussed in this work consider the plane passing through the center of the neutralizer cathode and the axis normal to the grids of the GIT. Notably, in the case of the axisymmetric simulation, the grid axis displayed with a black dotted line in Figure 1 becomes the axis of symmetry of the problem, so that only the lower half of the sketch should be considered. Clearly, from a geometrical stand point, this implies the assumption of an annular cathode. The body of the RIT10-EVO roughly has a total diameter of 15 cm, at the center of which the acceleration grid is located. Ions are only injected from an inscribed circle at the center of this grid, since its outer portion is composed of solid metal devoid of extraction holes. The outer edge of the thruster is encircled by a cylindrical wall which protrudes into the simulation domain. The thruster body and cylindrical walls are drawn in green in Figure 1, while the punctured and solid portions of the grid are shown respectively in light and dark red. The neutralization of the plume is guaranteed by an externally mounted cathode, oriented towards the plume by an angle of roughly 45°.

In our simulations we take the thruster potential as the reference one (i.e. $\phi_B = 0$) and define the other potentials in the simulation with respect to it. As a consequence, in order to impose a floating thruster configuration, the chamber walls must collect a zero net current ($I_{iW} + I_{eW} = 0$) at steady-state. This is obtained by varying, at each time step k, the potential of the facility walls ϕ_W.

$$\phi_W^{(k+1)} = \phi_W^{(k)} + \frac{1}{C}\left(I_{iW}^{(k)} + I_{eW}^{(k)}\right)\Delta t, \tag{1}$$

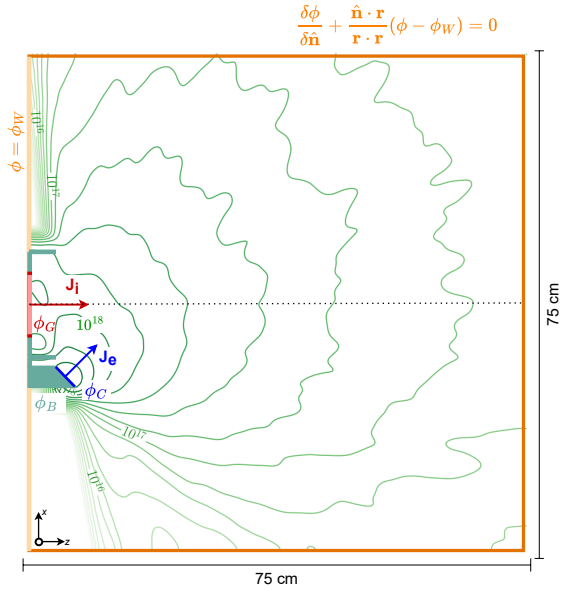

Figure 1: Sketch of the simulation domain. The ion and electron injections are depicted respectively in red and blue, while the green isolines display in m^{-3} the neutral density map obtained with the hybrid code EP2PLUS for the planar case.

so as to converge at steady-state to a current free plume, and a numerical value of the facility potential with respect to the thruster body. With regards to the thruster components, the RIT10-EVO was operated with an acceleration grid potential of $\phi_G = -150\,\mathrm{V}$, while a cathode extraction plate potential $\phi_C = 0\,\mathrm{V}$

The plasma in the RIT10-EVO plume is assumed to be composed of (i) Xenon neutral atoms, injected by the external grid of the thruster and the cathode, or present in the facility background; (ii) singly charged Xenon ions, injected through the thruster grid or produced in the plume; and (iii) electrons introduced from the cathode or generated by ionization inside of the domain. The injection of all of these species is carried out by assuming a Maxwellian distribution in their respective source, and introducing in the simulation domain only the forward-marching portion of this VDF. Table 2 summarizes the properties defining these injection Maxwellians for each plasma species, as well as the assumptions made in the characterization of the neutral population responsible for the facility background pressure. All of these values were chosen in accordance with the typical operating point of the thruster. Reasonable assumptions were made where no data was available (e.g. sonic neutral velocity, ion temperature, etc.). Note in particular that the ions' axial velocity at injection was chosen to respect the potential drop of 1150 V imposed between the thruster's grids, the ion flux corresponds to the nominal beam current of 0.1 A under the assumption of singly charged ions, and the properties of the background neutrals were chosen to provide a background pressure of 5×10^{-7} mbar.

B. Description of the Neutral Population

A fully self-consistent modelling of neutral particles is a particularly challenging aspect in full-PIC simulations of plasma plumes. The characteristic time of the neutral dynamics, in fact, is orders of magnitude larger than the simulation time step imposed by stability considerations on the characteristic electron frequencies. Worse still, the time required to consistently simulate the build-up of the facility background pressure, through the modelling of collisions, ion neutralization at the chamber walls, and the action of the facility pumps, pushes the time to steady-state to prohibitively large values for a PIC code. To avoid this large computational burden, the PIC simulations presented in this work do not evolve the neutral population in time, but employ constant density, velocity and temperature maps for its description. Specifically, two distinct set of maps are used. The first, representing the facility background population of neutrals, are uniform and constant maps of density, velocity and temperature with the values shown in Table 2. The

Species	Property	Value	Unit
Ions	Flux	9.82×10^{19}	$m^{-2}s^{-1}$
	Axial velocity	41137	m/s
	Temperature	0.1	eV
	Current	0.1	A
Thruster Neutrals	Flux	4.39×10^{19}	$m^{-2}s^{-1}$
	Axial velocity	300	m/s
	Temperature	0.0345	eV
Electrons	Flux	1.5×10^{21}	$m^{-2}s^{-1}$
	Axial velocity	0	m/s
	Temperature	3	eV
	Current	0.3	A
Cathode Neutrals	Flux	1.13×10^{21}	$m^{-2}s^{-1}$
	Axial velocity	300	m/s
	Temperature	0.0345	eV
Background Neutrals	Density	10^{16}	m^{-3}
	Temperature	0.0345	eV

Table 2: Injection properties of the species composing the plasma plume.

second is instead obtained by simulating the problem described in Subsection A with the in-house hybrid code for plume studies, EP2PLUS.[9,27] Thanks to a simplified quasi-neutral fluid description of electrons, closed at the momentum equation by means of a polytropic law, steady-state maps of the injected neutral population can be obtained with a reduced computational cost. The neutral properties employed in the full-PIC simulations thus represent the steady-state equilibrium between the expansion of neutrals injected from the cathode and through the thruster grids, and the effects of depletion through collisional processes such as ionization or resonant charge exchange. The neutral density map obtained with EP2PLUS is displayed with density isolines in Figure 1, and the interested reader may refer to Appendix A for further details on the most relevant plasma properties obtained with the hybrid simulation. Finally, we note here that previous works, that modelled in a fully consistent manner the build-up of the neutral population responsible for a facility's background pressure, have indeed obtained neutral density maps that agree well with the present approach of overlapping an injected neutral population to a uniform background density further away from the thruster.[3,8]

C. The PIC/MCC Formulation

The in-house code PICASO[28] has been employed for the full-PIC simulations of the GIT plume presented in this work. PICASO is a 2D3V, explicit, momentum-preserving PIC code that makes use of standard algorithms for the movement and weighing of the electron and ion macro-particles in a uniform, rectangular mesh. The classical Boris leapfrog algorithm[29] is in fact used to advance particles in two spatial and three velocity space dimensions, a first order could-in-cell shape function is employed for the particle weighing and the reconstruction of the species' macro-properties at the mesh nodes,[30] and a linear interpolation scheme allows the retrieval of the electromagnetic fields acting on each particle. The electric potential values at all domain nodes are obtained through the solution of Poisson's equation

$$\varepsilon\nabla^2\phi = -\rho_{el} \tag{2}$$

by means of its spatial discretization through second order finite difference schemes, and the resolution of the linear system thus obtained with Intel's MKL Pardiso solver.[31] Here $\rho_{el} = e(n_i - n_e)$ is the local space charge, and ε the electric permittivity.

The solution of Eq. (2) requires the imposition of boundary conditions at all simulation boundaries. In the case of the thruster components, their potentials ϕ_B, ϕ_C, and ϕ_G are imposed as Dirichelet conditions at the corresponding nodes. The vacuum chambers typically used for plume investigations, however, results too big to be entirely simulated in PICASO with reasonable computational expenses. As a consequence, the condition to be imposed at the domain edges results of more complex determination, as the domain must be inevitably cut short of the chamber walls, where it would be most natural to impose ϕ_W as BC. In order to truncate the domain before the facility walls, therefore, the Robin boundary conditions

$$\frac{\partial \phi}{\partial \hat{\mathbf{n}}} + \frac{\hat{\mathbf{n}} \cdot \mathbf{r}}{\mathbf{r} \cdot \mathbf{r}} (\phi - \phi_W) = 0 \tag{3}$$

proposed by Andrews *et al.*,[24] and based on the approximation of a monopole decay of the electric potential far from the plume's bulk, are employed at all downstream boundaries (in dark orange in Figure 1). Here ϕ is the potential at the boundary node, $\hat{\mathbf{n}}$ is the outward versor normal to the boundary, and $\mathbf{r}$ is the distance between the boundary node and a reference position, which is taken at the center of the acceleration grid. While these conditions were shown to hold at boundaries that do not contain the reference node, we maintain that their imposition on the upstream boundary, may be inaccurate. At this surface, in fact, the monopole term in the multipole expansion employed in the derivation of Eq. (3) is multiplied by $\mathbf{r} \cdot \hat{\mathbf{n}} = 0$, so that the higher order terms of the expansion may not be neglected. We prefer therefore to directly impose the facility wall potential as a Dirichlet condition at this upstream boundary (highlighted in light orange in Figure 1).

The BCs proposed by Andrews *et al.* also require an energy based evaluation of all particles crossing the downstream boundaries. It is in fact possible that, in reality, the direction of motion of charged particles is inverted back towards the plasma source downstream of the domain boundaries, so that they ultimately return back into the domain. These returning particles are fundamental to obtain quasi-neutrality in the plume bulk, and should not be eliminated from the simulation domain to avoid incurring in the electron pump instability.[23] The normal kinetic energy of all particles crossing the downstream boundaries is therefore evaluated, and compared with the potential energy required to reach the facility walls

$$\frac{1}{2} m (\mathbf{v} \cdot \hat{\mathbf{n}})^2 \geq Ze(\phi_W - \phi). \tag{4}$$

Note that here m represents the mass of the single physical particle, Z its charge number, e the elementary charge, and $\mathbf{v}$ the velocity vector of the macro-particle. If Eq.(4) is respected and the kinetic energy of the particle is sufficient to reach the chamber walls, it is removed from the simulation. If, on the other hand, Eq. (4) is false, and the particle results trapped in the plume's potential well, then it is specularly reflected back into the domain. For completeness, note that all particles that cross any other domain boundary are simply removed from the simulation.

Finally, Table 3 summarises the collisional operators considered in this work, detailing also the modelling strategy employed and the source of the data for the collision cross sections. In order to spare computational power, the multiple possible excited states of Xenon have been lumped in a single operator, characterized by an average cross section and energy threshold. Moreover, all collisions with neutrals have been modelled with the Monte Carlo Collision approach, neglecting any form of depletion of the neutral density that some of these collisions would entail (e.g. CEX or ionization collisions) as the neutral maps employed already consider these effects in their steady-state equilibrium. The electron-ion Coulomb collisions, on the other hand, are modelled with a DSMC operator that employs an analytical determination of the collision cross section based on the classical Coulomb collision theory.[32]

D. Electron and Ion Populations

Previous kinetic studies of GIT plumes have highlighted the possible presence of trapped and free electrons.[3,37] These electron classes subdivide the total electron population based on the total in-plane energy of each particle $\mathcal{E} = \frac{1}{2} m_e (v_x^2 + v_z^2) - e\phi$ with respect to the minimum energy required to exit the domain through one of its boundaries $\mathcal{E}_{ex} = -e \times max\{\phi_W, \phi_B, \phi_C, \phi_G\}$. If $\mathcal{E} < \mathcal{E}_{ex}$, in fact, the considered electron does not have sufficient energy to reach one of the domain boundaries, and results 'trapped' inside of the plume's potential well. On the other hand, electrons with sufficient total energy to leave the domain are termed 'free electrons'. In order to study in detail the properties of these two electron classes we subdivide them in separate electron lists inside of the code, so as to compute the macroscopic magnitudes of both

Collision	Species	Model	Data	Ref.
Elastic	e - n	MCC	E	[33]
Ionization	e - n	MCC	E	[33]
Excitation	e - n	MCC	E	[33]
Coulomb	e - i	MCC	A	[32]
CEX	i - n	DSMC	E	[34]
Elastic	i - n	MCC	E	[35]

Table 3: Description of the models used for the collisional events considered in the simulation. E points to the use of cross section data measured experimentally, while A refers to the use of an analytical model for the determination of the collision frequency. All data is taken from LXCat,[36] but references to the specific databases are also provided.

electron classes independently. All electrons are therefore initially injected in the free electron list (note, in fact, that electrons born at the cathode with a non-zero velocity always have $\mathcal{E} > -e\phi_C$). Every 100 simulation time steps, however, the code loops over the free electron list, and sorts those electrons with $\mathcal{E} < \mathcal{E}_{ex}$ into the list of trapped electrons.

Similarly, ions have also been subdivided into two separate lists: 'fast ions' and 'slow ions'. The former are all ions injected at high velocities through the thruster grids, while the latter are all of those ions produced inside of the plume either by ionization or CEX collisions. The 'slow ions', therefore, are generated with energies similar to those of their parent neutral, and are consequently more prone to a trajectory inversion back towards the thruster under the effects of the electric field. It is then convenient to sort them in a separate list in order to allow a more precise study of their interaction with the thruster and spacecraft. Finally, note that ions undergoing elastic or Coulomb collisions with neutrals and electrons are left in their original list, since in this case their energy is not altered as significantly as for ionization and CEX events.

E. Considerations on Numerical Parameters

Stability criteria for explicit momentum-conserving PIC codes impose limitations on the cell size Δl and time step Δt. In particular, for the unmagnetized plasma at hand, the most restrictive conditions require that the cell size results smaller than the Debye length λ_D throughout the domain, and that the time step is sufficiently small to accurately discretize the electron plasma frequency ω_{pe}. Imposing a minimum of 10 time steps for each electron plasma frequency oscillation, and considering the most restrictive value of the Debye length, this gives

$$\Delta l < \lambda_{D,min}, \qquad \Delta t < 0.1\omega_{pe}^{-1}. \tag{5}$$

These constraints can result excessively computationally taxing for the considered plasma properties, and as a consequence we resort to the artificial increase of the characteristic length and time scales of our problem through an augmentation factor f_D. This is carried out by employing an augmented electric permittivity $\varepsilon = f_D^2\varepsilon_0$ in Eq. (2), that substitutes the vacuum permittivity physically present in Poisson's equation and relaxes the numerical constraints of our problem. In the present work we employ an augmentation factor $f_D = 20$, which falls well within the range $f_D = 10 - 40$ used in other studies,[24,38,39] and which is expected to only increase the characteristic size of the Debye sheaths in the domain, without affecting significantly the physics of the plasma expansion.

In order to set the numerical parameters of our simulations we can obtain from the injection properties of Table 2 a characteristic plasma density $n^* = 2.4 \times 10^{15}$ m^{-3}, corresponding to the ion density at injection, and a reference temperature $T^* = 3$ eV. These yield an augmented Debye length $\lambda_D = 5.3$ mm, and a reduced electron plasma period $\omega_{pe}^{-1} = 7.2 \times 10^{-9}$ s, so that we may confidently choose a cell size $\Delta l = 3$ mm and a time step $\Delta t = 2 \times 10^{-10}$ s for our simulations. Finally, simulations were stopped after a total time $t_s = 3 \times 10^{-4}$ s, corresponding to 15 times the average ion transit time. Notwithstanding the apparently large value of t_s, it will be shown in the next Sections that some of the physical properties of the problem display an asymptotic behaviour in time, and that the simulations presented have approached but have not fully reached stationary conditions in this simulation time.

III. The General Plasma Response

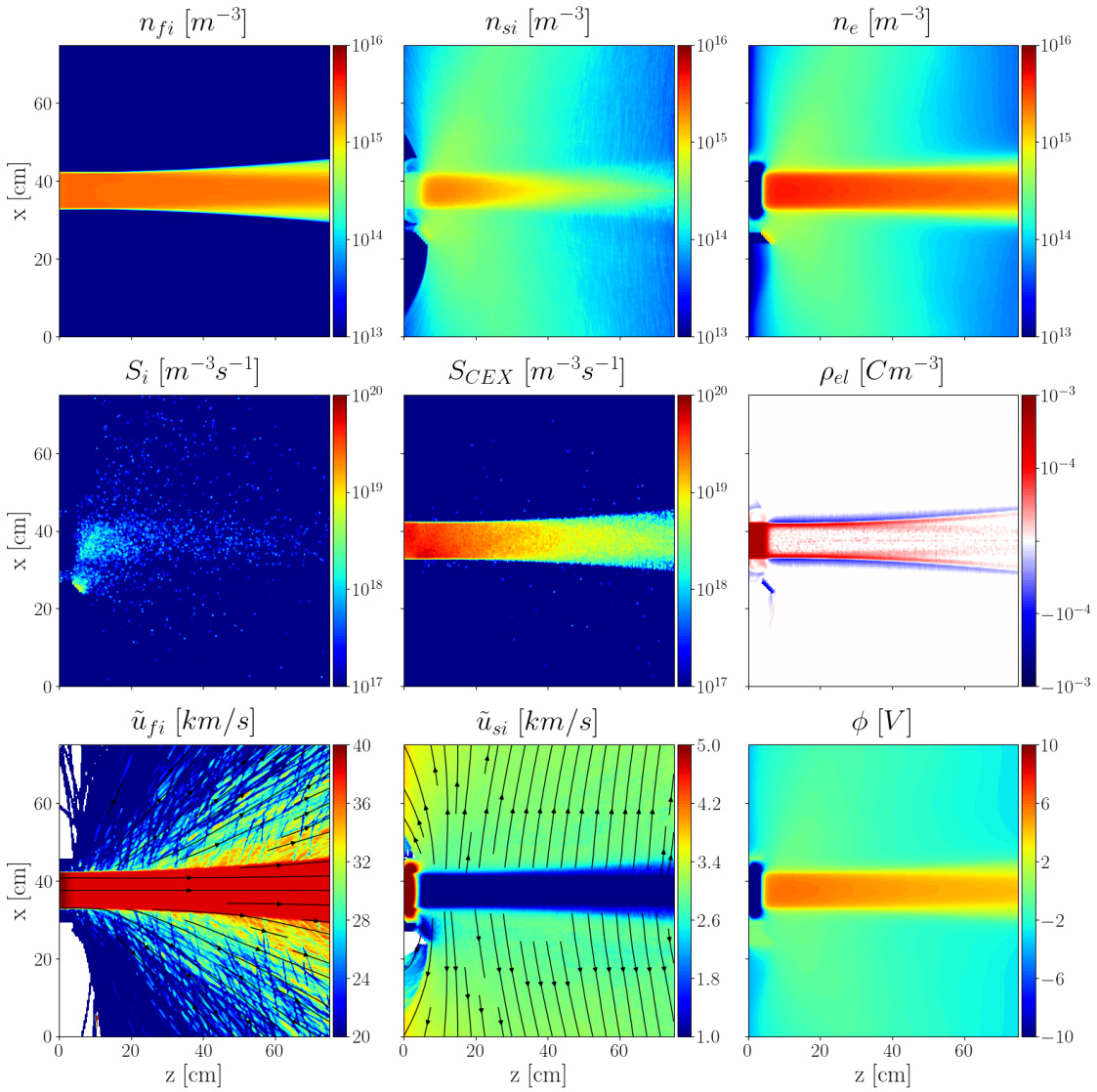

Figure 2: Plasma properties at the end of the reference simulation.

The Panels of Figure 2 show the plasma properties averaged over the final 70000 time steps of the planar simulation of the GIT plume. As expected, the most prominent features of the plume are defined by the highly inertial population of fast ions, which form the axial plasma beam visible in all Panels. Because of their large initial velocity, in fact, these ions traverse the domain displaying a mild sensitivity to the lateral electric forces, that only cause the small plume divergence observed at high axial coordinates in Panels (a) and (g). Note here that the lateral streaks external to the main ion beam visible in Panel (g) are due to those few fast ions that undergo elastic collisions. Axially, fast ions only suffer a relevant variation in velocities in the first few centimeters of the plume, in front of the acceleration grid (note the transition from a darker to a lighter red in Panel (g)). In fact, because the acceleration grid of the RIT10-EVO is directly exposed to the plasma plume, its very negative voltage causes the formation of a Debye sheath in front of it, visible both in the local absence of electrons shown in Panel (c), and in the strongly positive space charge displayed in Panel (f). The plasma potential consequently rises across the sheath by roughly 156V, decelerating the axial motion of fast ions.

Observing the electric charge density of Panel (f) it is clear that the bulk of the ion beam, downstream of the Debye sheath in front of the grids, is mainly quasi-neutral. Space charge is in fact principally present

at its edges, with electrons charging negatively the outer part of the plume boundary, and ions predominant at the inner edge. This lateral profile of the electric charge density causes, through Eq. (2), the lateral drop observed in the electric potential map of Panel (i) when moving from the center of the plasma beam to the outer edges of the domain. On the other hand, at the center of the plume and downstream of the initial potential rise, a negligible electric charge is found, leading to a very mild axial drop in the potential. As will be discussed later, this potential profile, characterized by a maximum value some centimeters downstream of the thruster grids, is responsible for the trapping of electrons inside of the plasma plume, and for the acceleration of slow ions laterally and upstream back towards the thruster.

The map of the electric charge in Panel (f) also highlights the presence of a strong negative charge in front of the cathode. The electron current injected from the cathode in this simulation, in fact, is three times larger than the ion current emitted through the acceleration grid. As a consequence, because we impose a current free plume at the downstream boundaries, a potential drop develops just in front of the cathode that allows a current $I_e = I_{i\,inj}$ composed of the most energetic electrons to proceed from the cathode into the plume, and reflects the less energetic ones back towards the cathode or the thruster body. This energetic mechanism for the selection of the electron current capable of entering the plume makes the choice of the electron flux injected by the cathode, which is an input parameter of the model, particularly challenging. In fact, any electron current $I_{e\,inj} > I_{i\,inj}$ inserted in the domain will yield a current free plume, since any electrons injected in excess will be deflected back to the cathode or thruster walls. Additionally, experimental measurements of the cathode currents do not provide valuable data in this sense, since these measurements also include the contributions of electrons returning from the plume to the cathode and therefore often yield cathode currents very similar to the ion current flowing through the grids. For this reason Section V presents the sensitivity of the simulation results to, amongst other input parameters, the injected electron current.

Figure 2(b) highlights how the population of slow ions represents a relevant portion of the total ion density in the domain, and even constitutes half of the total ion density a few centimeters downstream of the acceleration grid. By considering the ionization and CEX production rates for this class of ions (respectively in Panels (d) and (f)) it is clear that the vast majority of these ions are produced through CEX collisions, and that ionization could be freely neglected in the description of this population. Nevertheless, Panel (h) shows how both CEX and newly ionized ions produced downstream of the grid's Debye sheath undergo a relevant lateral acceleration caused by the potential drop at the edges of the fast ion beam. This process forms the characteristic CEX wings at the edges of the plume, populated by slow ions and electrons. More importantly, from the point of view of the lifetime of the acceleration grid, slow ions produced inside of the grid's Debye sheath are accelerated back towards it by the strong potential slope present here, and can impinge on the grid with energies of up to 157 eV.

IV. Free and Trapped Electrons

The first and second rows of Figure 3 display respectively the macroscopic properties of the free and trapped electron populations. The comparison between the two density plots (Panels (a) and (e)) immediately shows that the bulk of the ion beam is predominantly neutralized by trapped electrons, which represent more than 90% of the total electron population along the plume axis. Considering that all electrons injected at the cathode are initially free, since they have at least the energy necessary to return to the cathode or to the thruster body, an energy loss mechanism must exist that causes the progressive trapping of these electrons. Indeed, two mechanisms in our simulations are capable of reducing an electron's energy, causing it to be listed as trapped: ionization and excitation collisions, and the temporal variation of the electric potential during the initial transient. In the former case of inelastic collisions, colliding electrons provide part of their kinetic energy to excite or extract the electrons in the orbitals of the target neutral atoms, effectively decreasing their total energy and possibly causing them to be trapped in the plume. In the specific case of ionization collisions, not only is the energy of the parent electron reduced when providing a portion of the ionization energy, but a second electron may be produced inside of the plume's potential well, resulting in its immediate trapping. On the other hand, the total energy of electrons is only conserved under the hypothesis of a time-invariant electric potential, so that it is possible that initially free electrons undergo a decrease in their total energy during the initial transient, essentially trapping them in the developing potential well.

Once the total in-plane energy of an electron becomes low enough for it to result trapped, very few escape mechanisms are available for it to exit the simulation domain, and it can potentially remain inside of the plume forever. This is confirmed by the in-plane fluxes of trapped electrons shown in Figure 3(f),

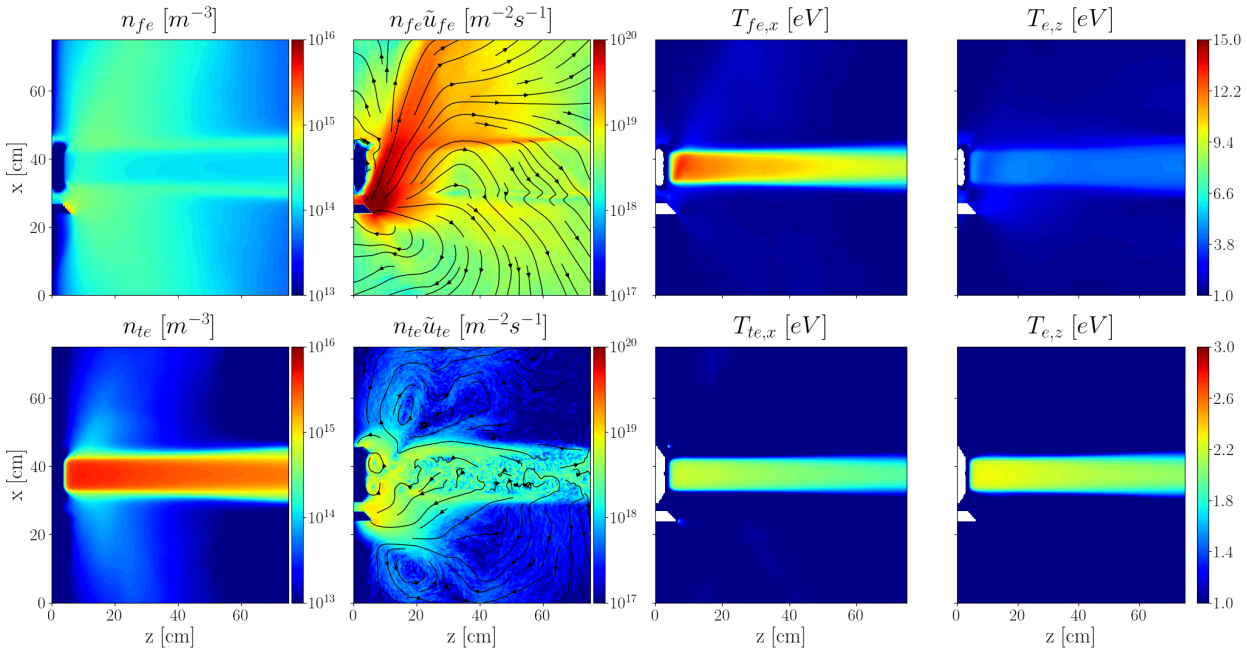

Figure 3: Properties of the free electron (upper row) and trapped electron (bottom row) classes for the reference simulation. Note the change of scales between the colour-maps of the free and trapped electron temperatures.

which displays negligible flows to any of the domain boundaries, and by Table 4, which reports the signed total currents of trapped and free electrons flowing to each domain boundary as a fraction of the injected ion current (positive when electrons are absorbed by the surface, negative when emitted). Additionally, no coherent structure can be identified in the streamlines at the center of the plasma beam when observing the plot of the trapped electron fluxes. The dense column of trapped electrons at the center of the plume is therefore essentially static, and is agitated only by a slight chaotic motion. Note that, although collisional events between these electrons and the ions and neutrals in the plume are infrequent, the trapped electron population results thermalized, because of their large (virtually infinite) residence time. This is evidenced by the isotropy of the temperature tensor, whose in plane, diagonal components are shown in Panels (g) and (h). Finally, it is interesting that the population of trapped electrons results roughly isothermal at the center of the plume, with $T_{te} \approx 2eV$, and relevantly colder than the population of free electrons (consider also the change in the scale of the colour maps between the plots of free and trapped electron temperatures). This rather low value of T_{te} is likely set by the energy threshold for ionization or excitation collisions: trapped electrons with sufficiently high kinetic energies will sooner or later undergo an inelastic collision, lowering their energy and consequently removing any high energy particle from the trapped electrons VDF.

	$I_{fe}/I_{i\,inj}$	$I_{te}/I_{i\,inj}$
Thruster Body	0.003	0.034
Grid	0.0	0.0
Cathode	-1.11	0.086
Chamber walls	0.96	0.013

Table 4: Free and trapped electron currents to the different domain boundaries expressed as a fraction of the ion current injected through the thruster grids. Negative values indicate a net electron flux emitted by the boundary, positive values indicate a net absorption of electrons.

Although the residence time of trapped electrons in the plume is importantly increased with respect to that of free electrons, the former do posse a few escape mechanisms. The first is linked to the fact that the

present simulation is bi-dimensional in space, but three-dimensional in velocity. As a consequence, electrons that undergo a collisional event that scatters the direction of their velocity vector may trade part of their out-of-plane kinetic energy for an increase of the in-plane kinetic energy, which could now result sufficient to escape the plume's potential well. It is worth noting that the inverse process may also lead to the trapping of free electrons, by tilting their in-plane velocity in the out-of-plane direction. However this latter case is statistically less probable, as there are two useful directions for electron escape (x and z) and only one for electron trapping (y). The second mechanism for the escape of trapped electrons is once again the time-variation of the electric potential. As we will later discuss with the use of Figure 4 the potential values in the plume bulk (and in particular the maximum potential value ϕ_{max}, found ∼9 cm downstream of the acceleration grid) gradually decrease over the course of the simulation. As a result the trapping potential drop also decreases, allowing an outflow of what were previously the most energetic trapped electrons. These escape mechanisms are likely the explanation for the moderate trapped electron flux observed to reach the cathode in Figure 3(f) and Table 4. Indeed the cathode is the domain boundary surrounded by the largest plasma density and with the highest electric potential, and represents as a result the easiest escape route for any trapped electron that has undergone an increase in its total in-plane energy.

Free electrons, on the other hand, consist of those particles that are injected by the cathode and never undergo a sufficient energy loss to cause their trapping inside of the plume. A portion of these electrons, indeed, never reach the ion plume, as their downstream motion is halted by the potential drop located in front of the cathode, and inverted back upstream where they neutralize on the cathode or thruster walls. This causes the density peak just in front of the cathode observed in Figure 3(a). The majority of the electrons with sufficient energy to overcome this initial potential rise are instead accelerated into the plume by the positive electric charge of the ion beam. Here, because of the large local neutral density and the recent gain in kinetic energy, a portion of these electrons undergo those inelastic collisions responsible for the production of trapped electrons. The others, instead, either cross the potential drop at the top of the plume and reach the upper domain boundary (see Panel (b)), or are reflected back into the plume. This latter portion of free electrons remain inside of the ion beam, bouncing against its lateral edges until they reach the downstream boundary or return to the cathode and exit the simulation. This is evidenced both by the local maxima in the free electron density at the lateral edges of the plasma beam in Panel (a), and by the large component of the free electron temperature tensor along x, symptom of the large spread of electron velocities in this dimension produced by their bouncing motion. Note that $T_{fe,z}$ is about half of the magnitude of $T_{fe,x}$, pointing to a strong anisotropy in the free electron class. Finally, it is important to consider that the potential of the facility walls ϕ_W is mostly influenced by the properties of this electron class, and is largely insensitive to the characteristics of trapped electrons. Indeed the total electron current to the facility walls I_{eW} in Eq. (1) is mostly comprised of free electrons, as clearly demonstrated by Table 4.

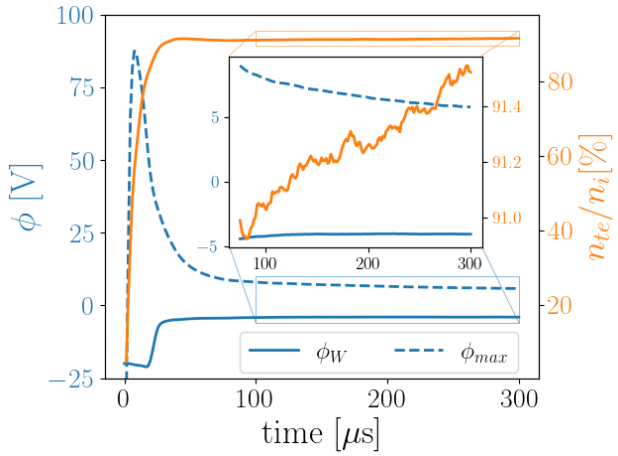

Figure 4: Convergence in time of the facility wall potential, maximum potential value in the plume bulk, and fraction of trapped electrons for the reference simulation.

The steady-state of the simulation requires that an equilibrium is reached between the trapping and escape mechanisms described above, that determine the properties of the trapped electron population. This

is a non-trivial process that may be better understood with the use of Figure 4. Here we show the temporal variation of the potential at the chamber walls with a continuous yellow line, and the maximum of the potential along the plume axis (which is roughly located at $x = 37.5\,\mathrm{cm}$, $z = 9\,\mathrm{cm}$) with a dashed yellow line. In blue, instead, we plot the ratio between the density of trapped electrons and the total density of ions around the point of maximum potential. The inlaid plot shows a zoom of the behaviour of these values in the last two thirds of the simulation, when the results are close to convergence. It is apparent from this graph that the value of ϕ_{max} and the fraction of trapped electrons present in the plume bulk are intimately linked. During the initial transient, in fact, as the ion beam creates a region of highly positive electric charge in front of the thruster grids, the plume potential rises to values close to $\phi_{max} = 90\,\mathrm{V}$. This produces a strong potential ramp that accelerates free electrons generated at the cathode towards the center of the ion beam with very high energies, which lead to the profuse ionization of the neutral atoms emitted by the thruster and the production of numerous trapped electrons. As the ratio of trapped electrons increases, they contribute to the neutralization of the ion beam, reducing the electric charge and consequently the value of the electric potential in the plume. This in turn diminishes the energy of the free electrons arriving into the plume and the ionization rate, slowing down the trapped electron production. Nevertheless, the inlaid plot shows that, by the end of the simulation, the equilibrium between trapping and escape mechanisms for trapped electrons has not yet been completely reached, since the number of these electrons is still slowly increasing and the maximum plume potential displays a gradual decline. Eventually an equilibrium condition will however be obtained, in which any newly produced trapped electrons will cause a consequent drop of the plume's potential and the release of an equal number of electrons, leading to no changes in the overall properties of the plume. It is important to consider that this asymptotic approach to equilibrium is characterised by a timescale linked to the inelastic collision frequency, which at low electron energies may result very slow, but should not be overlooked in the attempt to reduce the simulation's computational times. Finally note that the potential of the facility walls does converge to a constant value within the simulation time. As mentioned, in fact, ϕ_W is mainly determined by the free electrons, and is therefore less affected by the slow build up of the trapped electron population.

These considerations highlight the importance of the inclusion of trapping mechanisms in simulations of the neutralization of GIT ion beams. Indeed, the underestimation of the trapped electron population leads to an overestimation of the potential rise in front of the grids of the GIT, which in previous works has led to excessively large electron temperatures and to an increase in the beam divergence caused by the deceleration of ions at the thruster exhaust.[3,18] Additionally, Kozakov *et al.*[37] have recently shown that the trapped electron population may pose challenges also for experimental investigations. Intrusive probing of the plume, in fact, may provide an additional escape mechanism for electrons, which may now neutralize at the probe's surfaces. If the generation of trapped electrons is sufficiently slow this may strongly alter their equilibrium, depleting their population in the plume and causing an increase in the potential values in front of the thruster. This in turn can vary the general plume properties measured.

V. Sensitivity Analysis

The previous Section has highlighted the importance of inelastic collisions in the plasma response. In order to confirm the physical mechanisms identified previously we present here an additional simulation, where we neglect ionization and excitation collisions. Moreover, the present Section aims to study the sensitivity of the simulation results to some critically unknown input parameters of the model, such as the current and the temperature of the electrons injected by the cathode into the domain. As a result, two further simulations have been considered, in which the cathode current and the electron temperature have been respectively doubled to $I_{e\,inj} = 0.6\,\mathrm{A}$ and $T_e = 6\,\mathrm{eV}$. Figure 5 compares the results of these three additional simulations with the reference one by plotting the densities and scalar temperatures of free and trapped electrons, together with the electric potential and the electric charge density. These quantities are shown along the plume axis in the first and third column, and in the lateral direction, 37.5 cm downstream of the thruster grids, in the second and fourth columns. Here the results relative to the reference simulation are plotted in blue, while the cases with double the electron temperature, double the electron injection current and no inelastic collisions are respectively shown in yellow, red and green. To provide further information useful for the discussion of these results Table 5 also displays the steady-state values of the chamber potential for each simulation.

The first thing that is immediately evident from Figure 5 is the strong discrepancy in all the plotted

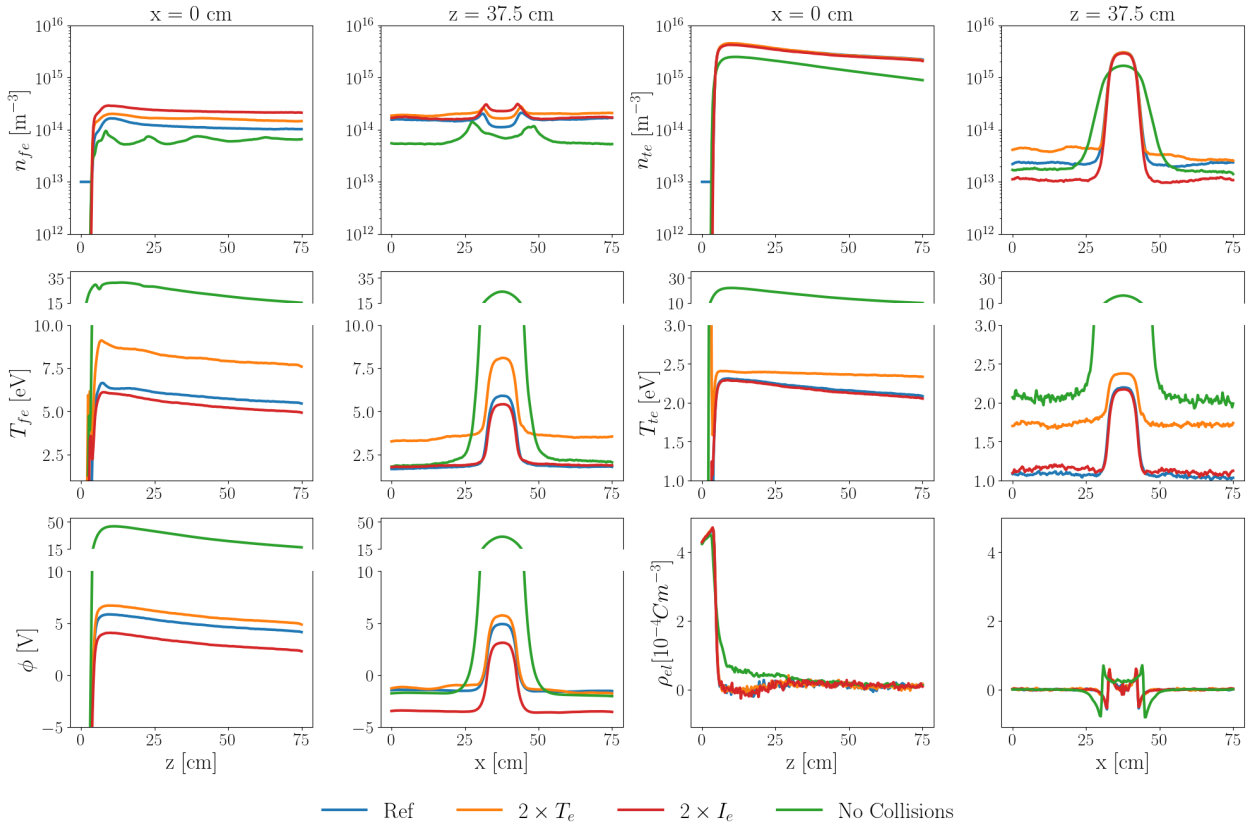

Figure 5: Comparison of the most relevant plasma properties obtained for the simulation scenarios considered along the ion beam axis and in the lateral direction at the center of the domain.

values between the simulation with no inelastic collisions and the other cases, to the extent that a break in the abscissas of the temperature and potential plots was required for visualization purposes. The cause of this variation has already been introduced in the previous Sections: the absence of inelastic collisions removes one of the most prominent electron trapping mechanisms, strongly reducing the trapped population as shown by Panels (c) and (d). This in turn leads to a reduced neutralization of the ion beam (note the positive electric charge present well downstream of the ion optics in Panel (k)) and a hefty increase in the plume's electric potential (see Panel (i)). The result is that fast ions undergo a stronger deceleration in front of the thruster grids, leading to the larger plume divergence observable in all plots of the second and fourth columns. Moreover, the free electrons accelerated into the plume gain a large amount of kinetic energy from the strong potential rise between the cathode and the plume bulk, which translates into the considerable values of the free electron temperature observed in Panels (e) and (f). Once accelerated into the plume, a portion of the free electrons may bounce on the plume edges, moving with a zig-zag motion downstream. This kind of bouncing trajectory is present also in the collisional cases, but is damped out by the inelastic collisions and by the gradual energy loss of these electrons that eventually fall into the trapped class. As a consequence, the density peaks, that are observed only for the collisionless case in the axial free electron density of Panel(a), indicate the positions where the beam of bouncing free electrons crosses the plume axis. Similarly to free electrons, trapped electrons for the collisionless case also display a substantial scalar temperature, which can be attributed to the large trapping potential drop found at the edges of the plume, capable of trapping electrons with a wide spread of velocities. Finally, note that the facility wall potential shown in Table 5 for this case is nearly identical to the one obtained with the reference simulation. As already mentioned, in fact, the value of ϕ_W is strongly insensitive to the trapped electron properties, which is the electron class most affected by the exclusion of inelastic electron collisions. In fact, while the maps of the free electron properties vary due to the changes in the potential profiles in the domain, the total energy of each free electron, which is what determines whether it reaches the chamber walls or not, is essentially

Case	ϕ_W [V]
Ref	-4.02
$2 \times T_e$	-7.49
$2 \times j_e$	-6.30
No Collisions	-4.03

Table 5: Values of the facility wall potential for the simulation scenarios considered.

unaffected due to the conservative nature of the electric forces.

Conversely to the case with no inelastic collisions, the cases with a doubled electron temperature or current appear to influence mostly the properties linked to the free electron population, while leaving the characteristics of trapped electrons mostly unvaried. Panels (c) and (d), in fact, display a negligible variation within the main ion beam both in the axial and lateral profiles of the trapped electron density for these two cases. Similarly, also the trapped electron temperature shown in Panels (g) and (h) appears to be mostly insensitive to the injected electron current, and only mildly dependant on the injected electron temperature. Interestingly in this latter case the trapped electron population is essentially isothermal along the plasma plume, causing it to result progressively warmer than in the reference case as one moves downstream. These negligible variations in the trapped electron population cause an identical neutralization of the ion beam throughout all three simulations, as demonstrated by Panels (k) and (l), which leads to the very similar profiles of the electric potential observed in Panels (i) and (j). The upward or downward shifts of these profiles with respect to the reference simulation are instead linked to the free electron population. Note, in fact, that the free electron properties result directly connected with the injection parameters at the cathode: doubling the injection temperature causes the temperature values of free electrons to be roughly doubled (see Panels (e) and (f)), while increasing the injected current causes an increase in the free electron densities (Panels (a) and (b)). Because this electron class groups the more energetic electrons present in the domain, which are therefore capable of further penetrating inside the Debye sheaths found at the edges of the plasma plume (i.e. in front of the thruster grids and at the chamber walls), it is the one mostly responsible for the determination of the sheaths' potential drop. According to classical sheath theory, in fact, the potential drop in a Debye sheath is known to be proportional to the electron temperature, causing the increased potential rise in front of the acceleration grid for the simulation with the larger electron temperature, and as a consequence the upward shift of its potential profile with respect to the reference simulation. The larger electron temperature in this simulation also accentuates the average energy of the free electrons at the domain edge, explaining the low value of the chamber potential of Table 5 which is necessary to maintain the electron current to the walls equal to the ion one. A similar mechanism takes place for the case of the increased electron current, where more electrons must be reflected back into the domain at the outer boundaries to maintain $I_{eW} = I_{iW}$. This causes the decrease of the facility potential with respect to the reference case shown in Table 5, which in turn drags down the entire potential map decreasing the potential values in comparison to the reference scenario.

VI. Axisymmetric Simulation

The final objective of this research is to eventually compare the obtained numerical results with experimental data. In order to obtain a proper comparison with experiments, however, the simulation of a three-dimensional expansion will be necessary. Nevertheless, the employed PIC code PICASO is bi-dimensional in space, and we therefore make use of axisymmetric simulations to achieve a 3D expansion. While this implies the simulation of an annular cathode that surrounds the ion source, and the consequent loss of the asymmetry of the real system generated by the externally located cathode, we believe this to be an acceptable approximation for our purpose. Indeed, all of the previous bi-dimensional and asymmetric simulation results show that all asymmetry is lost immediately downstream of the cathode, and that the main bulk of the ion beam is perfectly symmetric. Analogously to the previous planar case, we therefore first ran a three-dimensional plume simulation in the hybrid code EP2PLUS to retrieve the neutral density map, which was then imported into PICASO. The simulation domain considered for the PIC simulation is the

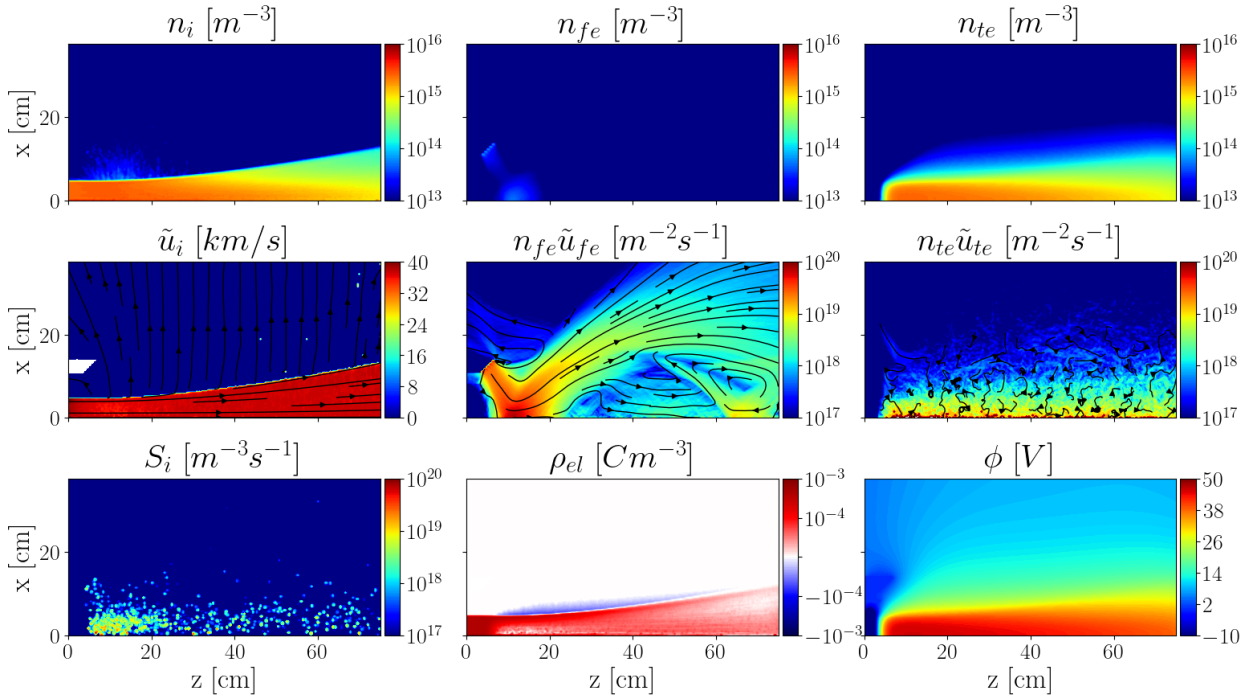

Figure 6: Plasma properties obtained at the end of the axisymmetric simulation case.

one shown in Figure 1 below the black dotted line (now representing the axis of symmetry), but the density map obtained for this 3D case is relevantly more sparse with respect to the one shown in the Figure because of the additional dimension of the expansion. All other simulation parameters are kept unchanged, except for the specific fluxes of the injected particles, which are re-scaled to maintain the ion, electron and neutral total flux unchanged even with the new injection surface areas given by the cylindrical geometry considered.

Figure 6 displays the axisymmetric simulation results. Two things immediately jump to the eye. The first is the increased divergence of the plume with respect to the planar case and the large potential values displayed in Panel (i). These latter are caused by the positive electric charge shown by Panel (h) in the plume bulk, which in turn is explained by considering the low trapped electron densities of Panel (c) when compared to the densities we had obtained for the previous cases. This is due to the much lower neutral density found in the plume in this axisymmetric case, which effectively reduces the probability of inelastic collisions and slows down the production of trapped electrons. Although Panel (g) displays an ionization source term which is comparable in magnitude to the one in Figure2, in fact, this ionization rate is obtained with relevantly more energetic free electrons, which are accelerated by the strong potential rise in the plume. Were the potential value to decrease, the free electron energy would also diminish, reducing the ionization frequency and essentially slowing down the approach to steady-state. As a result, after 0.3 ms, this axisymmetric simulation is even further from steady-state than the one presented in Section III. As for the collisionless case of Section V, the large potential rise that this incomplete neutralization of the ion beam causes in front of the thruster grid leads to the deceleration of the fast ion population, and the increase of the plume's divergence.

The second thing immediately noticeable in Figure 6, is the very low density of the free electrons displayed in Panel (b). Similarly to the case of the neutral density, this is simply explained by considering the additional direction of expansion that is now available to these electrons. While fast ions and trapped electrons essentially form a mono-dimensional beam, neutrals, slow ions and free electrons are free to expand in all directions, causing a relevant decrease in their density when moving from a 2D to a 3D expansion.

Apart from these two exceptions, the axisymmetric simulation qualitatively behaves analogously to what has already been discussed for the planar cases. Fast ions are slightly decelerated in the Debye sheath in front of the grids, and then continue their axial motion, while slow ions are accelerated laterally (see the total ion velocities of Panel (d)). Free electrons accelerate through the ion beam and then reach the chamber walls on

the opposite side (Panel (e)), and the trapped ones only display a chaotic motion inside of the plume's bulk (Panel (f)). We note here, as a final remark, a variation in the chamber potential for this axisymmetric case, which at the end of the simulation yields $\phi_W = 5.6\,\mathrm{V}$. While this result better approaches the experimental measurements of this value, a steady-state simulation is required before the comparison with experimental data may be confidently undertaken.

VII. Conclusions

In this work we have employed our in-house 2D PIC code PICASO to simulate the expansion of Ariane's RIT10-EVO gridded ion thruster. Importantly, these simulations consider an extensive library of collisional processes, including inelastic electron collisions such as ionization and excitation of the fluid neutral background. These collisions were observed to be crucial in the formation of a trapped electron population, which allowed a much more efficient neutralization of the ion beam and the consequent decrease of the large potential values observed in previous publications in front of the thruster grids. This in turn allowed a decrease in the divergence of the plasma plume and simulation results that better resemble those measured experimentally.

Additionally, using an energy-based criterion the trapped and free electrons in the simulations were subdivided into separate particle lists, allowing a more precise study of the macroscopic properties of each population. Free electrons were found to be noticeably more energetic than their trapped counterparts, and resulted responsible for the generation of the trapped electron population principally through ionization, and for the determination of the floating thruster potential. Conversely trapped electrons had relatively moderate and isotropic temperature values, and resulted mainly responsible for the neutralization of the plasma plume and the formation of the plume's potential profile. Moreover, this latter population was observed to be largely insensitive to variations of the cathode injection properties, but displayed a slow approach to a steady-state equilibrium which was strongly governed by the inelastic collisions included in the simulations.

Finally the preliminary results of an axisymmetric simulation, more suitable for the comparison with experimental data, were presented. This simulation displayed many of the characteristics of the planar case analysed previously, but also showed a much slower approach to stationary conditions due to the much lower neutral density found in the plume when adding an additional dimension to the expansion. The low neutral density, in fact, caused a decrease in the electron collision frequencies, and therefore a slower build up of the trapped electron population necessary to fully neutralize the plume.

Acknowledgements

This work has been supported by the ECOMODIS project, funded by the European Space Agency, under contract 4000137869/22/NL/RA

A. Hybrid Simulation

Figure 7 shows the plasma properties obtained with the quasi-neutral, hybrid code EP2PLUS. Notice that, while qualitatively the plume shape and the ion fluxes appear to match the ones obtained with the non-neutral PIC code, the values of electric potential and the behaviour of the electron currents result quite different. Moreover, it is interesting to note that, because the code is quasi-neutral, the Debye sheath in front on the thruster grids is here assumed infinitesimal, and described by means of an analytical model.

References

[1]K Holste, P Dietz, S Scharmann, K Keil, T Henning, D Zschätzsch, M Reitemeyer, B Nauschütt, F Kiefer, F Kunze, et al. Ion thrusters for electric propulsion: Scientific issues developing a niche technology into a game changer. *Review of Scientific Instruments*, 91(6):061101, 2020.

[2]W.R. Kerslake and L.R. Ignaczak. Development and flight history of the SERT II spacecraft. *J. Spacecr. Rockets*, 30:258–290, 1993.

[3]Keita Nishii and Deborah A Levin. Kinetic simulation of ion thruster plume neutralization in a vacuum chamber. *Plasma Sources Science and Technology*, 2023.

[4]John E Foster and Tyler J Topham. A review of the impact of ground test-related facility effects on gridded ion thruster operation and performance. *Physics of Plasmas*, 31(3), 2024.

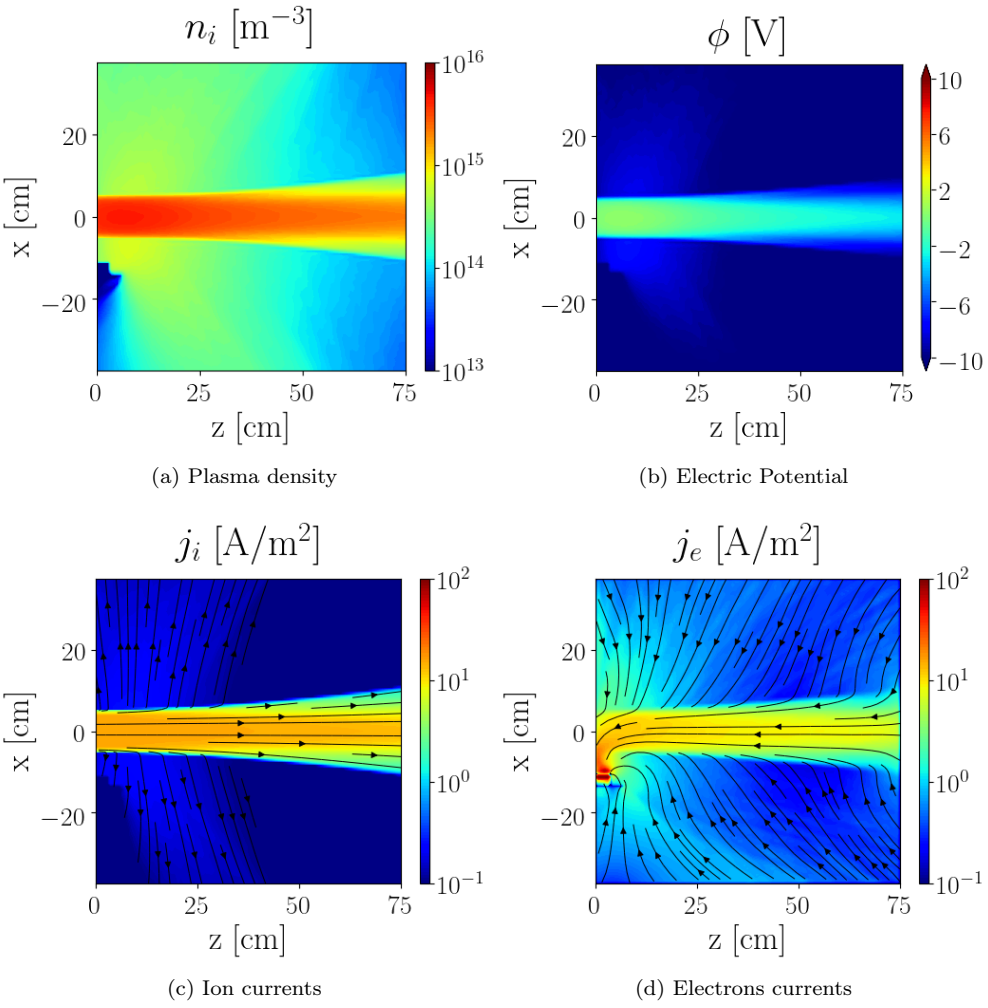

(a) Plasma density

(b) Electric Potential

(c) Ion currents

(d) Electrons currents

Figure 7: Plasma properties obtained with the quasi-neutral hybrid code EP2PLUS

[5]B. Korkut and D.A. Levin. Three dimensional DSMC-PIC simulations of ion thruster plumes with SUGAR. In *50th Joint Propulsion Conference*, paper 2014-3447, Cleveland, Ohio, July 28–30, 2014. American Institute of Aeronautics and Astronautics, Reston, VA.

[6]B. Korkut, Z. Li, and D.A. Levin. 3-D simulation of ion thruster plumes using octree adaptive mesh refinement. *IEEE Transactions on Plasma Science*, 43(5):1706–1721, 2015.

[7]Burak Korkut and Deborah A Levin. Three-dimensional simulations of backflows from ion thruster plumes using unstructured grid refinement. *Journal of Propulsion and Power*, 33(1):264–275, 2017.

[8]Burak Korkut, Deborah A Levin, and Ozgur Tumuklu. Simulations of ion thruster plumes in ground facilities using adaptive mesh refinement. *Journal of Propulsion and Power*, 33(3):681–696, 2017.

[9]Filippo Cichocki, Adrián Domínguez-Vázquez, Mario Merino, and Eduardo Ahedo. Hybrid 3D model for the interaction of plasma thruster plumes with nearby objects. *Plasma Sources Science and Technology*, 26(12):125008, 2017.

[10]Hideyuki Usui, Akihiko Hashimoto, and Yohei Miyake. Electron behavior in ion beam neutralization in electric propulsion: full particle-in-cell simulation. In *Journal of Physics: Conference Series*, volume 454, page 012017. IOP Publishing, 2013.

[11]Y. Hu and J. Wang. Electron properties in collisionless mesothermal plasma expansion: Fully kinetic simulations. *IEEE Transactions on Plasma Science*, 43(9):2832–2838, 2015.

[12]Y. Hu and J. Wang. Fully kinetic simulations of collisionless, mesothermal plasma emission: macroscopic plume structure and microscopic electron characteristics. *Physics of Plasmas*, 24(3):033510, 2017.

[13]J. Wang, O. Chang, and Y. Cao. Electron-ion coupling in mesothermal plasma beam emission: Full particle PIC simulations. *IEEE Transactions on Plasma Science*, 40(2):230–236, 2012.

[14]J. Wang, D. Han, and Y. Hu. Kinetic simulations of plasma plume potential in a vacuum chamber. *IEEE Transactions on Plasma Science*, 43(9):3047–3053, 2015.

[15]N. Nuwal, R. Jambunathan, and D. Levin. Kinetic modeling of spacecraft surfaces in a plume backflow region. *IEEE Transactions on Plasma Science*, 48(12):4305–4325, 2020.

[16]R. Jambunathan and D.A. Levin. Kinetic modeling of plasma plumes using multi-gpu forest of octree approach. In *35th International Electric Propulsion Conference*, 2017.

[17]R. Jambunathan and D. A. Levin. Chaos: An octree-based pic-dsmc code for modeling of electron kinetic properties in a plasma plume using mpi-cuda parallelization. *Journal of Computational Physics*, 373:571–604, 2018.

[18]R. Jambunathan and D. A. Levin. A self-consistent open boundary condition for fully kinetic plasma thruster plume simulations. *IEEE Transactions on Plasma Science*, 48(3):610–630, 2020.

[19]R. Jambunathan and D. A. Levin. Kinetic, 3-d, pic-dsmc simulations of ion thruster plumes and the backflow region. *IEEE Transactions on Plasma Science*, 48(6):2017–2034, 2020.

[20]Keita Nishii and Deborah A Levin. Three-dimensional kinetic simulations of carbon backsputtering in vacuum chambers from ion thruster plumes. *Journal of Propulsion and Power*, pages 1–15, 2023.

[21]Y. Zhao, J. Wang, and H. Usui. Simulations of ion thruster beam neutralization using a particle–particle model. *Journal of Propulsion and Power*, 34(5):1109–1115, 2018.

[22]Min Li, Mario Merino, Eduardo Ahedo, and Haibin Tang. On electron boundary conditions in PIC plasma thruster plume simulations. *Plasma Sources Science and Technology*, 28(03):034004, 2019.

[23]L. Brieda. Model for steady-state fully kinetic ion beam neutralization studies. *IEEE Transactions on Plasma Science*, 46(3):556–562, 2018.

[24]Shaun Andrews, Simone Di Fede, and Mirko Magarotto. Fully kinetic model of plasma expansion in a magnetic nozzle. *Plasma Sources Science and Technology*, 2022.

[25]PCT De Boer. Electric probe measurements in the plume of an ion thruster. *Journal of propulsion and power*, 12(1):95–104, 1996.

[26]Konstantin Keil, Kristof Holste, and Peter J. Klar. Multi-diagnostics system in the jumbo space simulation test facility in giessen, germany. In *Proc. 38th Int. Electric Propulsion Conference*, 2024.

[27]Alberto Modesti, Filippo Cichocki, and Eduardo Ahedo. Numerical treatment of a magnetized electron fluid model in a 3d simulator of plasma thruster plumes. *Frontiers in Physics*, 11, 2023.

[28]Alberto Marín-Cebrián, Enrique Bello-Benítez, Adrián Domínguez-Vázquez, and Eduardo Ahedo. Macroscopic response of a Hall thruster discharge from an axial-radial PIC model. In 76^{th} *Gaseous Electronics Conference*, Ann Arbor, MI, October 9-13, 2023.

[29]R.W. Hockney and J.W. Eastwood. *Computer simulation using particles*. CRC Press, Boca Ratón, FL, 1988.

[30]C.K. Birdsall and D. Fuss. Clouds-in-clouds, clouds-in-cells physics for many-body plasma simulation. *Journal of Computational Physics*, 135(2):141–148, 1997.

[31]oneMKL PARDISO - Parallel Direct Sparse Solver Interface. `https://www.intel.com/content/www/us/en/docs/onemkl/developer-reference-c/2023-1/onemkl-pardiso-parallel-direct-sparse-solver-iface.html`. Accessed: 2023.

[32]R.J. Goldston and P.H. Rutherford. *Introduction to Plasma Physics*. Institute of Physics Publishing, Bristol, 1995.

[33]Biagi database. `https://nl.lxcat.net`. Accessed: 2019-10-23.

[34]J.S. Miller, S.H. Pullins, D.J. Levandier, Y. Chiu, and R.A. Dressler. Xenon charge exchange cross sections for electrostatic thruster models. *Journal of Applied Physics*, 91(3):984–991, 2002.

[35]A.V. Phelps. Technical report 28. *JILA Information Center Report, University of Colorado, Boulder, Colorado, US*, 1985.

[36]L.C. Pitchford et al. Lxcat: an open-access, web-based platform for data needed for modeling low temperature plasmas. *Plasma Process and Polymers*, 14:1600098, 2017.

[37]Ruslan Kozakov, Maximilian Maigler, Jochen Schein, and Neil Wallace. Determination of self-neutralization phenomena of ion beams with langmuir probe measurements and pic-dsmc simulations. *Applied Sciences*, 14(8):3470, 2024.

[38]Alberto Marín-Cebrián, Enrique Bello-Benítez, Adrián Domínguez-Vázquez, and Eduardo Ahedo. Non-maxwellian electron effects on the macroscopic response of a hall thruster discharge from an axial–radial kinetic model. *Plasma Sources Science and Technology*, 33(2):025008, feb 2024.

[39]Tiannan Yuan, Junxue Ren, Jun Zhou, Zhe Zhang, Yibai Wang, and Haibin Tang. The effects of numerical acceleration techniques on pic-mcc simulations of ion thrusters. *AIP Advances*, 10(4):045115, 2020.